Mater. Res. Soc. Symp. Proc. Vol. 920 © 2006 Materials Research Society 0920-S01-05

Drawing of Hollow Multilayered All-Polymer Fibers

Elio Pone, Charles Dubois, Ning Guo, Yan Gao, Alexandre Dupuis, Suzanne Lacroix, and Maksim Skorobogatiy
École Polytechnique de Montréal, Montréal, Québec, H3C 3A7, Canada

ABSTRACT

We present a fluid dynamics model for the drawing of hollow multilayer polymer optical fiber. A newtonian model is considered assuming slender geometries. Hollow core collapse during drawing and layer thickness non-uniformity are investigated as a function of draw temperature, draw ratio, feeding speed, core pressurization and mismatch of material properties in a multilayer.

INTRODUCTION

Hollow core multilayer and microstructured optical fibers (MOF) for radiation guiding in the near and mid-infrared (IR) [1-11] have recently received close attention as they promise considerable advantage over their solid core counterparts in applications related to power guidance at almost any IR wavelength for military, industry and medical applications, IR imaging and sensing, and even THz transmission. Due to its complexity, fabrication of such waveguides is an active field of research. Four main methods have been identified for hollow core fiber manufacturing, each offering its own advantages and challenges. First method is a deposition of metallo-dielectric films on the inside of a drawn capillary by liquid-phase coating [5,6]; technical challenges in enforcing thickness uniformity in the resultant coatings limit fiber length to the distances of 10m. Second method is a capillary stacking method [7-9] where glass capillaries are arranged in a periodic manner and then drawn; so far such fibers have been mostly demonstrated to guide below $3\mu m$ due to the non-transparency of silica and polymer materials used in the fabrication. Third method is a deposition of radially uniform thin films on a drawn substrate fiber by means of physical or chemical vapor deposition methods [10]; main challenge of this technology is presumably uniformity of the resultant coatings, and a throughput due to a relatively slow deposition process. Finally, film rolling process [11] starts with a deposition of a glass (chalcogenide) film on top of a polymer film with consecutive rolling around a mandrel tube, tube etching and drawing; potential challenges include fiber profile optimization which is somewhat nontrivial due to a strictly periodic reflector geometry imposed by the fabrication method, another potential challenge is controlling bio-compatibility of a resultant fiber.
In our research group we study fabrication of all-polymer hollow multilayer fibers. Although refractive index contrast between layers in an all-polymer Bragg fiber is relatively small (at most 1.3/1.7), as demonstrated in [12] liquid core all-polymer Bragg fibers can be designed to guide very well both TE and TM like modes, while gas filled all-polymer Bragg fibers can guide effectively a TE polarized mode. We believe that fabrication simplicity, and potential bio-compatibility of such fibers can be attractive for applications in bio-medical sector. Recently, our research group has succeeded in developing two methodologies for fabrication of multilayered

all-polymer hollow preforms. One approach uses consecutive deposition of layers of two different polymers by solvent evaporation on the inside of a rotating polymer cladding tube [13]. Orthogonal solvents were found, and solvent evaporation process was developed for both PMMA(Polymethyl methylacrylate)/PS(Polystyrene) and PVDF(Polyvinylidene fluoride)/PC(Polycarbonate) material combinations. In Figure 1(a), a 30cm long all-polymer preform of 10 consecutive PMMA/PS layers deposited on the inside of a PMMA cladding tube is presented, while in Figure 1(b) preform crossection is shown. Alternative method uses a co-rolling of two dissimilar polymer films similarly to [11]; in Figure 1(c), a 20cm long all-polymer preform of 19 consecutive polystyrene PVDF/PC is presented, while in Figure 1(d) crossection of a drawn fiber is shown.

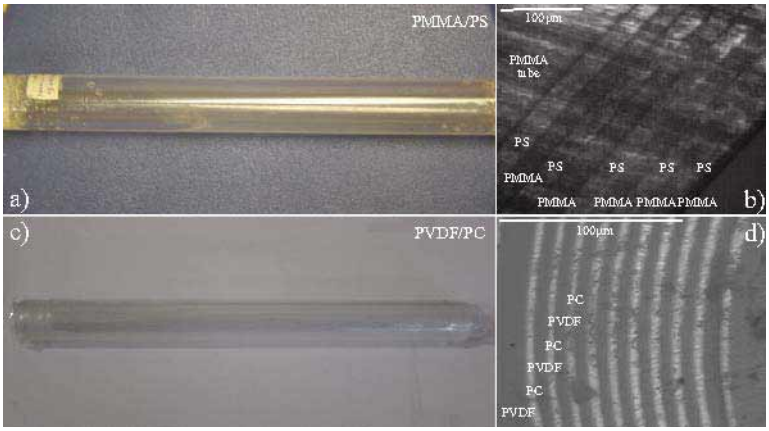

Figure 1. a) 30cm long all-polymer preform of 10 consecutive PMMA/PS layers deposited on the inside of a PMMA cladding tube b) PMMA/PS preform crossection c) 20cm long preform of 19 consecutive PVDF/PC layers d) crossection of a drawn PVDF/PC fiber.

After preform is fabricated, hollow MOFs are manufactured by preform heating and drawing. Geometry of the final fiber can be significantly influenced by controlling various parameters in the drawing process such as temperature distribution in a furnace, fiber drawing and preform feed velocities, as well as pressurization of the hollow core. Moreover, if several materials are used in a single preform, drawing process can be influenced greatly by the mismatch in the viscosities of the constitutive materials.

Previous studies on fiber drawing have focused mainly on spinning molten threadlines [14,15] or drawing conventional solid optical fibers [16,17]. Drawing of hollow fibers was first studied in [18] where the asymptotic "thin-filament" equations were obtained but the effects of surface tension were neglected. A more complete analysis is given in [19-21].

When relatively high temperatures or low speeds are used, the surface tension force can be of importance and it can cause an partial or even complete collapse of the hollow core. This hole collapse affects not only the initial ratio between the inner and outer diameters of the preform but also the uniformity of layers thickness. The purpose of this paper is to characterize such a hole collapse during the drawing of hollow fibers when the surface tension effects are non negligible. In particular, we investigate how the hole collapse is affected by standard control parameters such as draw temperature, draw ratio, feeding speed, core pressurization and mismatch of material properties in a multilayer.

BASIC EQUATIONS

Schematic of a hollow multilayer preform profile during drawing is shown in Figure 2.

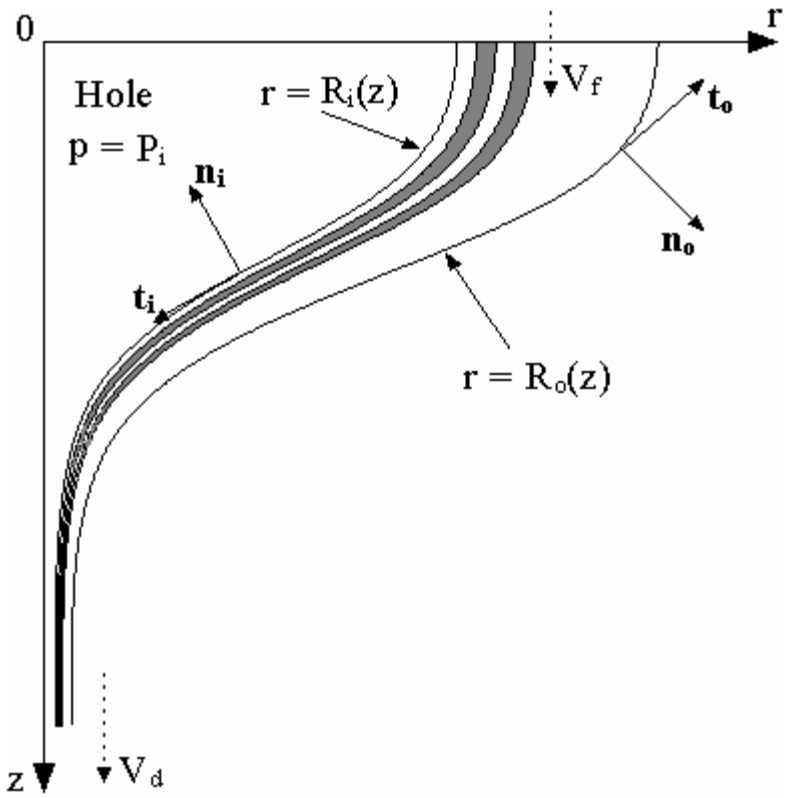

Figure 2. Schematic of a hollow multilayer preform during drawing. Different colors correspond to different materials in a multilayer.

For an incompressible axisymmetric steady flow the equations for conservation of mass and momentum in cylindrical coordinates are as follows:

$$\frac{1}{r}\frac{\partial(rv_r)}{\partial r}+\frac{\partial v_z}{\partial z}=0 \tag{1}$$

$$\begin{aligned}\rho\left(v_r\frac{\partial v_r}{\partial r}+v_z\frac{\partial v_r}{\partial z}\right)&=-\frac{\partial p}{\partial r}+\frac{1}{r}\frac{\partial(r\tau_{rr})}{\partial r}-\frac{\tau_{\theta\theta}}{r}+\frac{\partial\tau_{rz}}{\partial z}\\ \rho\left(v_r\frac{\partial v_z}{\partial r}+v_z\frac{\partial v_z}{\partial z}\right)&=-\frac{\partial p}{\partial z}+\frac{1}{r}\frac{\partial(r\tau_{rz})}{\partial r}+\frac{\partial\tau_{zz}}{\partial z}+\rho g\end{aligned} \tag{2}$$

where r and z are the radial and axial coordinates, v_r and v_z are the r and z components of the velocity vector $\mathbf{v}$, ρ is a constant density, p is a pressure, τ_{ij} is an extra-stress and g is a gravitational acceleration. The components of a total stress tensor $\bar{\bar{\sigma}}$ are

$$\sigma_{ij}=-p\delta_{ij}+\tau_{ij} \tag{3}$$

The definition of τ_{ij} depends upon the polymer model, and is discussed in details later. For these equations, we need to specify the boundary conditions. At the interfaces between different layers the kinematic conditions are

$$v_r = R'_j v_z \qquad \text{at} \qquad r = R_j \tag{4}$$

where $R_j = R_j(z)$ denote the interfaces between layers and the index $j = 1, 2 \ldots N$ is used to number them starting from the inner one. The primes denote the derivative with respect to z. Since the first and the *N*-th interfaces are external interfaces, we will distinguish them by denoting $R_i \equiv R_1$ and $R_o \equiv R_N$ for the inner and outer boundaries respectively.

Hollow core can be pressurized in order to control its collapse under the action of a surface tension. In this case, at the inner interface the dynamic boundary conditions are

$$\begin{aligned} \bar{\bar{\sigma}} \cdot \mathbf{n_i} &= \left(\gamma \kappa_i - P_i\right) \mathbf{n_i} \\ \bar{\bar{\sigma}} \cdot \mathbf{t_i} &= 0 \end{aligned} \tag{5}$$

where γ denotes the surface tension coefficient, and

$$\kappa_i = 1 R_i (1 + R'^{\,2}_i)^{1/2} - R''_i (1 + R'^{\,2}_i)^{3/2} \tag{6}$$

is the curvature, while P_i is the hole overpressure (constant ambient pressure has no effect on the flow). Outward-pointing normal at the inner boundary $\mathbf{n_i}$ is defined as:

$$\mathbf{n_i}^T = \left(n_r, n_\theta, n_z\right) = \left(-\frac{1}{\sqrt{1 + R'^{\,2}_i}}, 0, \frac{R'_i}{\sqrt{1 + R'^{\,2}_i}} \right), \tag{7}$$

while

$$\mathbf{t_i}^T = \left(n_z, 0, -n_r\right) \tag{8}$$

is the unit tangent vector. In a similar way, the dynamic boundary conditions at the outer boundary are

$$\begin{aligned} \bar{\bar{\sigma}} \cdot \mathbf{n_o} &= -\gamma \kappa_o \mathbf{n_o} \\ \bar{\bar{\sigma}} \cdot \mathbf{t_o} &= 0 \end{aligned} \tag{9}$$

where $\mathbf{n_o}$, $\mathbf{t_o}$ and κ_o satisfy the same equations as $-\mathbf{n_i}$, $-\mathbf{t_i}$ and κ_i respectively with R_i replaced by R_o.

At the interfaces between the internal layers, we will consider a continuous stress and velocity. In the axial direction the boundary conditions are the known values of the drawing (V_d) and the feeding (V_f) velocities. Furthermore, as an initial condition, the values $R_j(0)$ are known.

THIN FILAMENT EQUATIONS

One of the basic dimensionless parameters in the problem is the ratio between the preform radius and the length of the neck down region defined as ε. In the case when $\varepsilon << 1$ a so called *thin filament* approximation can be used. There are two different approaches for simplifying the equations in this case. In the first approach [19,22], the variables are expanded as power series in ε^2 and only the dominant terms are retained in the equations. In the second approach [18], which we also follow in this paper, the equations are averaged over the cross-section at each value of z.

The average $\bar{\varphi}(z)$ of a variable $\varphi(z)$ is defined as

$$\bar{\varphi}(z) = \frac{1}{\pi\left(R_o{}^2 - R_i{}^2\right)} \int_{R_i}^{R_o} 2\pi r \varphi(r,z) dr \tag{10}$$

For the axial velocity, the assumption $v_z = \bar{v}_z$ is made explicitly. We note first that for a slow varying thin filament; $R'_j << 1$, and by neglecting terms of the order R'^2_j the boundary conditions (5) and (9) take the following form:

$$\begin{aligned}
&\sigma_{rr} = \frac{\gamma}{R_i} - P_i && && \sigma_{rr} = -\frac{\gamma}{R_o} \\
&\sigma_{rz} = \left(-\frac{\gamma}{R_i} + P_i\right) R'_i && \text{at} \quad r = R_i && \sigma_{rz} = \frac{\gamma}{R_o} R'_o && \text{at} \quad r = R_o \\
&\sigma_{zz} = \left(\frac{\gamma}{R_i} - P_i\right) R'^2_i && && \sigma_{zz} = -\frac{\gamma}{R_o} R'^2_o
\end{aligned} \tag{11}$$

Multiplying the r-component of the momentum equation (2) by $2\pi r^2$, integrating from R_i to R_o, considering $\frac{d}{dz}\int_{R_i}^{R_o} 2\pi r^2 \tau_{rz} dr \approx 0$, neglecting the inertial term because of the small value of the radial velocity and using the boundary values of σ_{rr} given by (11), we obtain

$$\bar{p} = \frac{\bar{\tau}_{rr} + \bar{\tau}_{\theta\theta}}{2} + \frac{\gamma\left(R_o + R_i\right) - R_i^2 P_i}{R_o^2 - R_i^2} \tag{12}$$

Multiplying the z-component of the momentum equation (2) by $2\pi r$, integrating from R_i to R_o, using the boundary values of $\tau_{rz} = \sigma_{rz}$ given by (11) as well as the equation (12) and neglecting terms of relative order R'^2_j, we obtain

$$\bar{\rho} Q v'_z = \left[\frac{Q}{v_z}\left(\bar{\tau}_{zz} - \frac{\bar{\tau}_{rr} + \bar{\tau}_{\theta\theta}}{2}\right) + \gamma\left(R_o + R_i\right)\right]' + \bar{\rho} g \frac{Q}{v_z} \tag{13}$$

where $\pi Q = \pi\left(R_o^2 - R_i^2\right) v_z$ is the constant volumetric flow rate. This is the axial force balance equation.

NEWTONIAN FLOW

In general polymers are viscoelastic and the viscosity depends on the kinematics of the flow. But at high temperatures, for some polymers such as PMMA and PS, we can still consider a Newtonian model. The constitutive equation for the Newtonian fluid is

$$\bar{\bar{\tau}} = \eta(r,z)\left(\nabla \mathbf{v} + \nabla \mathbf{v}^T\right) \tag{14}$$

where η is the viscosity which in our case depends on r and z. In this paper we consider a uniform temperature in any given cross-section, thus T is only a function of z. We also assume an axial variation of the temperature dependent viscosity for each constituent material. From the continuity equation one finds:

$$v_r = -\frac{r v'_z}{2} + \frac{A}{r} \tag{15}$$

where $A = A(z)$ is a function to be determined later. The extra-stress tensor takes the form:

$$\overline{\overline{\tau}} = \begin{pmatrix} -\eta\left(v'_z + \frac{2A}{r^2}\right) & 0 & 0 \\ 0 & -\eta\left(v'_z - \frac{2A}{r^2}\right) & 0 \\ 0 & 0 & 2\eta v'_z \end{pmatrix} \tag{16}$$

where the component $\tau_{rz} = \eta \frac{\partial v_r}{\partial z}$ has been neglected. From (16) the following relation holds for the averaged components of an extra-stress tensor

$$\bar{\tau}_{zz} - \frac{\bar{\tau}_{rr} + \bar{\tau}_{\theta\theta}}{2} = 3\bar{\eta} v'_z \tag{17}$$

and the axial force balance equation (13) can be written in the form

$$\bar{\rho} Q v'_z = \left[3\bar{\eta} Q \frac{v'_z}{v_z} + \gamma\left(R_o + R_i\right) \right]' + \bar{\rho} g \frac{Q}{v_z} \tag{18}$$

The expression for A is obtained by directly integrating the r-component of the momentum equation (2) from R_i to R_o and using the boundary values of σ_{rr} given by (11)

$$A = \frac{P_i - \gamma\left(1/R_i + 1/R_o\right)}{4\int_{R_i}^{R_o} \frac{\eta(r)}{r^3} dr} \tag{19}$$

Combining the kinematic boundary conditions (4) with relation (15), we obtain

$$\left(R_j^2 v_z\right)' = 2A \tag{20}$$

NUMERICAL SOLUTION

The last three equations may be considered as a system of coupled differential equations for $v_z(z)$, $A(z)$ and $R_j(z)$. This system of equations can be solved with an iterative method. Starting from an arbitrary initial distribution of $v_z(z)$, say a linear distribution between the feeding and drawing speed, the initial value equations (20) can be integrated in order to obtain $R_j(z)$ with the value of A given by (19). This functions are then used to solve the boundary value problem (18) to obtain a new function $v_z(z)$ passing so at the next iteration. For the examples given later in this paper we have tested this procedure and it converges very fast (less than 200 iterations).

In most cases of practical importance, inertial, gravitational and capillary terms in (18) can be neglected and it takes a simple form

$$\bar{\eta} \frac{v'_z}{v_z} = C \tag{21}$$

where C is a constant. This equation, which is now uncoupled from the other two, can be easily integrated to give

$$v_z(z) = \exp\left(\ln V_f + \frac{\int_0^z \frac{dz}{\overline{\eta}(z)}}{\int_0^L \frac{dz}{\overline{\eta}(z)}} \ln \frac{V_d}{V_f} \right) \tag{22}$$

where L is a furnace length. Once the axial velocity is known, the initial value equations (20) can be easily integrated to obtain the profile of a drawn structure.

One of the key aspects of hollow preform drawing is the partial or even complete collapse of a compressible core as a result of the surface tension forces acting at the free boundaries. In what follows we characterize the hole collapse by the ratio $\frac{R_i^f}{R_o^f} / \frac{R_i^p}{R_o^p}$, where index f defines the drawn fiber, while index p defines the preform.

Hole collapse typically results in a faster reduction of a smaller core radius compared to the larger outer radius. Thus, starting with identical thicknesses of the same material layers in a preform, in a drawn fiber the inner layers will become thicker than the outer ones. We will characterize the thickness non-uniformity by the ratio $\frac{h_o}{h_i}$ between the thickness of the outer layer and the thickness of the inner one, assuming they were equal in a preform.

In the following we investigate how the hole collapse and layer thickness non-uniformity is influenced by various control parameters. As an example, we consider drawing of a multilayer hollow Bragg fiber preform where cladding tube and one of the two materials of a multilayer is PMMA, while the other material is a different polymer. Materials in consecutive polymer layers are alternated to create a periodic multilayer structure.

Effects of draw ratio, temperature and viscosity mismatch

In our calculations we assume a uniaxial temperature distribution with a maximum at the furnace center (Figure 3). In the following when we vary the maximum value of the temperature (T) we simply rescale the whole profile. We assume that Newtonian viscosity of PMMA obeys an Arrhenius type dependency [23]

$$\eta(T) = 1.506 \times 10^5 \exp\left[2935 \left(\frac{1}{T} - \frac{1}{170} \right) \right] \text{N.s/m}^2 \tag{23}$$

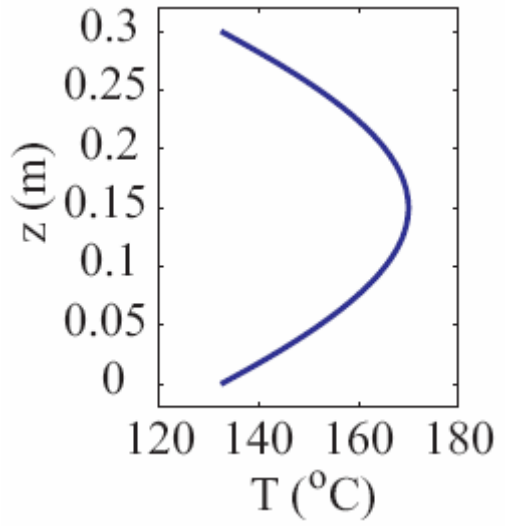

Figure 3. Temperature distribution in the furnace.

In our first calculation viscosity of the other polymer is assumed to be simply two times higher than that of PMMA. Although we recognize that to model correctly the flow of a particular polymer we need to use its proper temperature dependent viscosity, in our first simulation we rather want to highlight the major effect of adding another material into a preform. Particularly, we want to investigate how the core collapse is affected by the viscosity of the second material despite of its small volume fraction in the preform.

We consider drawing of a preform with external and internal diameter 31.75 and 25.4mm respectively. PMMA tube is coated on the inside with 25 alternated layers of PMMA and another polymer with a viscosity two times higher, each one of them having a thickness of 50 μ m. The value of surface tension coefficient is considered constant for exterior interfaces $\gamma = 0.032$ N/m [24] and both densities are considered to be 1195kg/m^3 [23]. We also assume a furnace length $L = 30$ cm, a constant preform feeding velocity $V_f = 2.5\mu$ m/s and a zero pressurization $P_i = 0$.

First, we consider the effects of varying the drawing ratio defined as $D_r = V_d / V_f$ and the maximum temperature in a furnace. In Figure 4(a), solid lines represent the parameter of a core collapse $\frac{R_i^f}{R_o^f} / \frac{R_i^p}{R_o^p}$ as a function of a draw ratio $D_r = V_d / V_f$ for different values of the maximal temperature. Dashed lines represent the parameter curves resulting in a constant outside diameter $D_o \equiv 2R_o = 125\mu m$ and $D_o = 250\mu m$ after the draw. For comparison, in dotted curves we present the core collapse if no other polymer is present in the preform (drawing of a simple PMMA tube of the same inner and outer radii as a multilayer preform).

We see that to prevent hole collapse higher draw ratios and lower temperatures have to be used. Both cases demand higher draw force which might lead to fiber breakage. We also observe that the collapse of the tube with the same thickness as the multilayer preform is more pronounced because of a lower average viscosity. Effect of the temperature on a core collapse is easy to understand as viscosity decreases rapidly with reduction of the temperature, thus hindering the hole collapse.

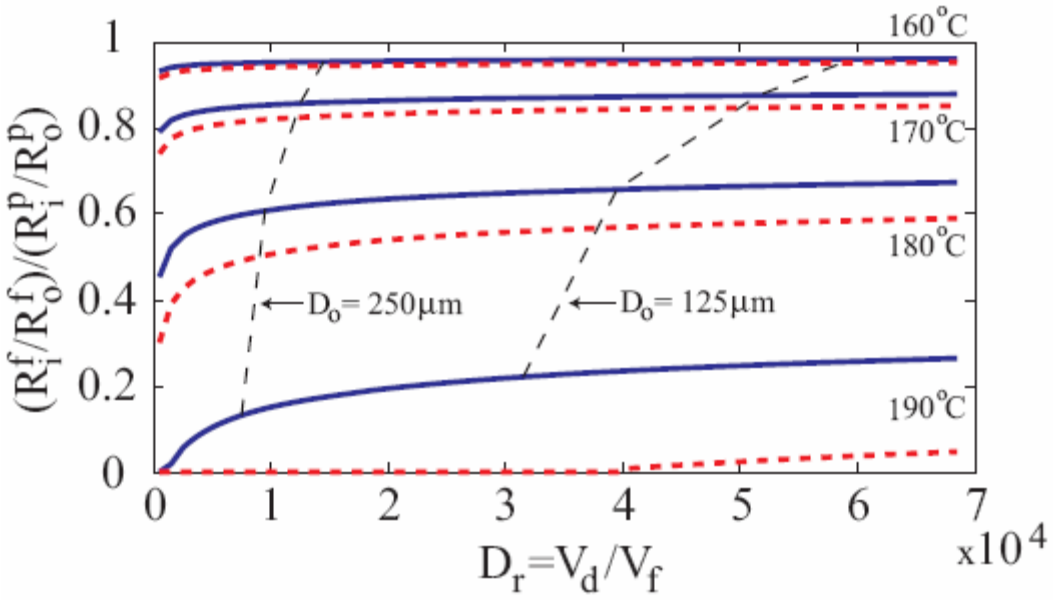

(a)

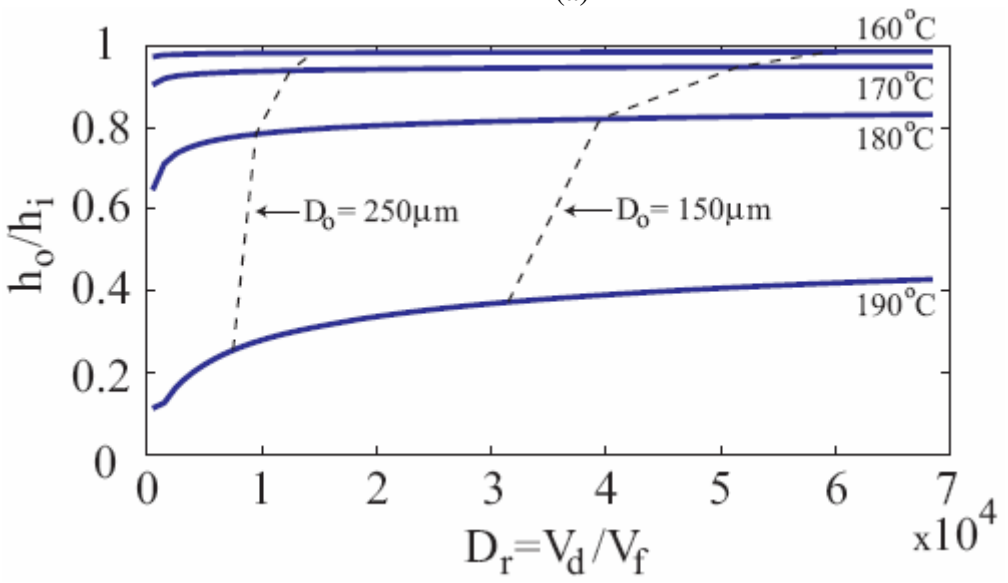

(b)

Figure 4. (a) Normalized ratio R_i/R_o as a function of a draw ratio D_r for different temperatures. Solid lines describe drawing of a multilayer preform. Dotted lines describe drawing of a simple tube having exactly the same dimensions as a multilayer preform. Dashed lines represent the curves of a constant outside diameter. (b) Ratio h_o/h_i between the inner and outer layer thicknesses as a function of the draw ratio for different temperatures.

Effect of the draw ratio is more subtle. Starting with preforms of the same diameter, draw ratio increase leads to the reduction of a resultant fiber cross-section. As a consequence, the forces of surface tension become more pronounced, thus favoring the hole collapse. This is overcompensated by the fact that increasing the draw ratio leads to the higher axial velocities, thus the time a cross-section spends in a melted zone diminishes which works against the hole collapse.

In Figure 4(b), thickness non-uniformity parameter is presented as a function of the draw ratio for different values of the maximum temperature. The curves are similar to those for the hole collapse in Figure 4(a). From mass conservation, the ratio between the cross-section areas of different layers remains constant from which it follows that the thickness non-uniformity parameter is proportional to the hole collapse.

We now describe in more details the effect of mismatch in the polymer viscosities when two different materials are used in the same preform. As seen in Figure 4(a), the hole collapse is considerably less pronounced for the multilayer structure despite the fact that the higher viscosity material occupies only a very small fraction of the total volume and its viscosity is only two times higher than that of PMMA. In what follows we assume that multilayer preform is made of PMMA and another polymer. For the viscosity of a second material similar Arrhenius law as for PMMA is assumed (23)

$$\eta(T) = \eta_0 \exp\left[\alpha\left(\frac{1}{T} - \frac{1}{T_0}\right)\right] \tag{24}$$

where η_0 and α are constant coefficients and T_0 is a reference temperature. First, we investigate the effects of changing η_0 while keeping the other parameters unchanged, which corresponds to the case of using the same polymer, but with a different molecular mass. Second, we investigate the effects of changing T_0 which corresponds to the case of varying the polymer material. In Figure 5, we consider drawing of preforms of various compositions at a fixed maximum furnace temperature of $190^{\circ}\mathrm{C}$ and a draw rate $D_r = 30000$. Multilayer preform geometry is the same as described above; mismatch in the polymer viscosities is described in terms of the ratios of the material parameters $\eta_0/\eta_{0,PMMA}$ and $(T_0 - T_{0,PMMA})/T_{0,PMMA}$. From Figure 5, we see that the hole collapse depends significatively on the viscosity of a second material and can be prevented by choosing a polymer with an appropriate viscosity.

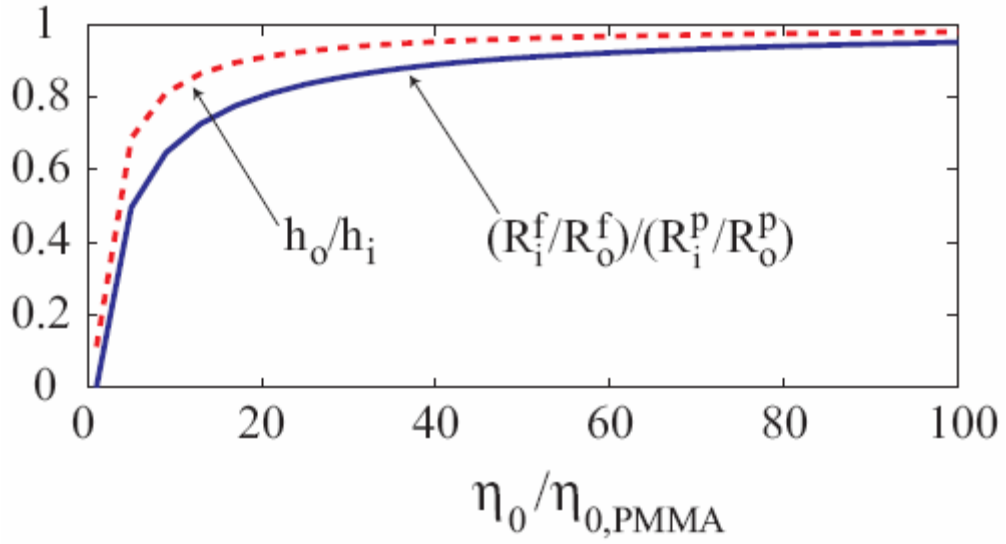

(a)

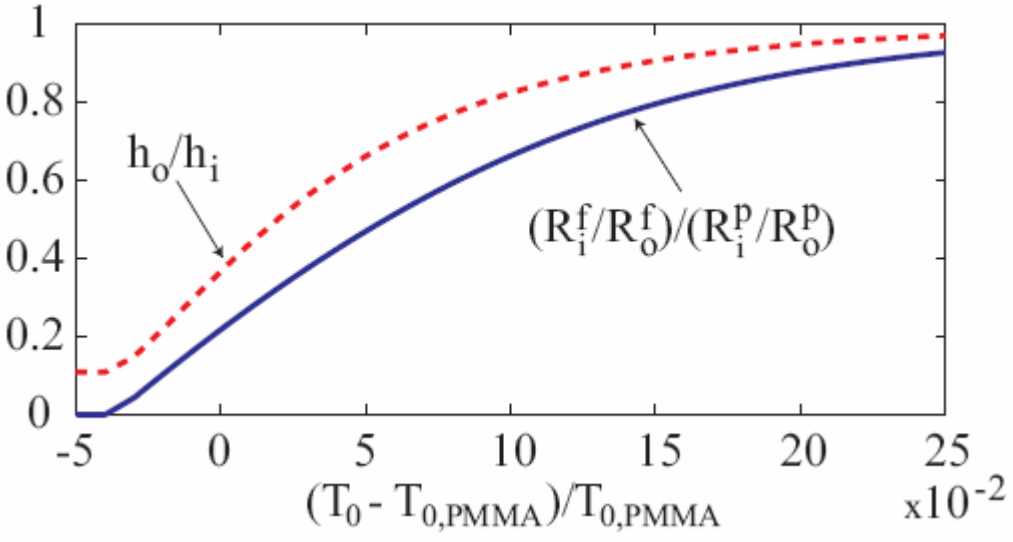

(b)

Figure 5. Effect of mismatch in the viscosities of materials in a multilayer on core collapse (solid lines), and layer non-uniformity (dotted lines).Maximum furnace temperature is $T = 190^{\circ}\mathrm{C}$, draw rate $D_r = 30000$.

Effects of the pressurization and preform feeding velocity

Other parameters that influence core collapse are the hole overpressure and the feeding speed. By increasing the hole pressure we expect to reduce the hole collapse. Also, for a given draw ratio, by increasing the preform feeding speed we expect reduction of the core collapse as fiber cross-section would spend less time in the melted zone.

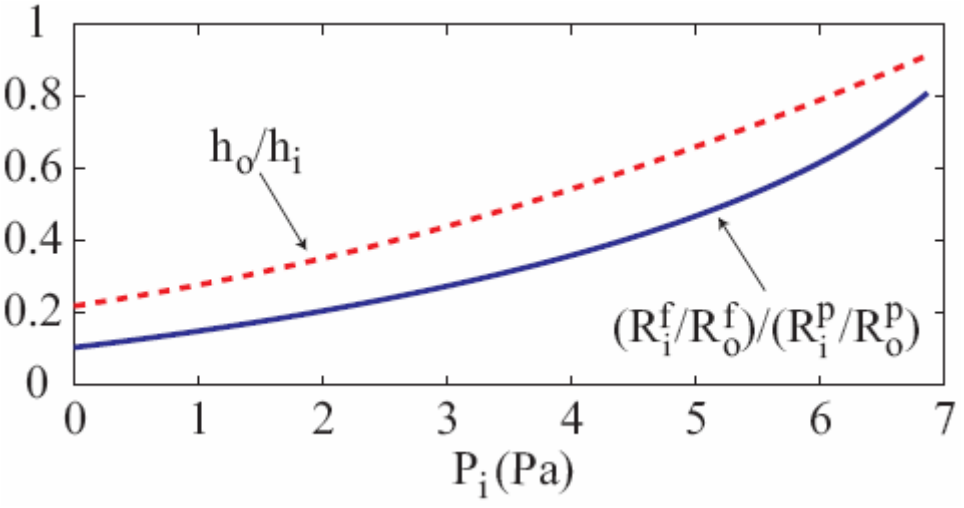

(a)

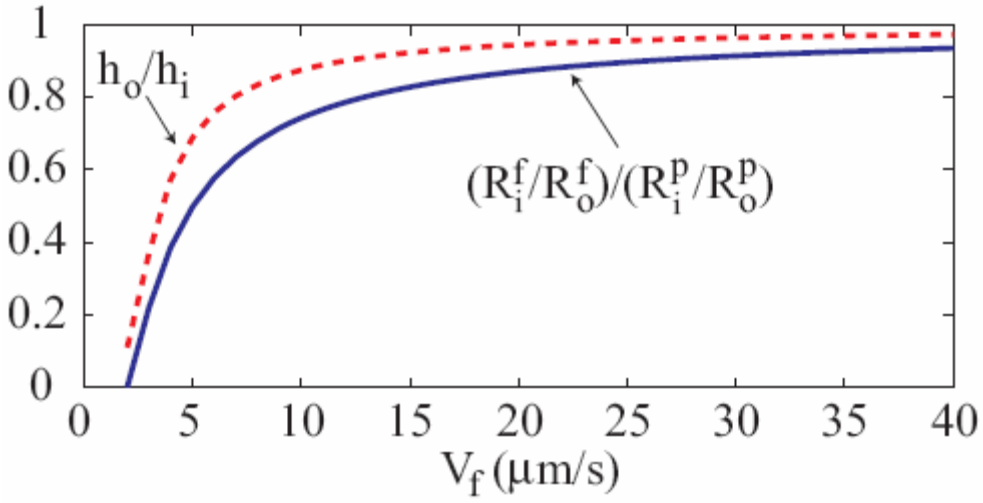

(a)

Figure 6. The hole collapse and thickness non-uniformity as a function of the hole overpressure (a) and feeding speed (b). Maximal furnace temperature is $T = 190^{\circ}\mathrm{C}$, draw rate $D_r = 5000$.

We consider drawing of the same preform as in a previous section using the draw ratio $D_r = 5000$, while the other draw parameters remain unchanged. In Figure 6, core collapse and layer thickness non-uniformity are presented as functions of the hole overpressure P_i and feeding speed V_f. As expected, the hole collapse is very sensitive to pressurization, and in principle, can be reduced by increasing the pressure. Time evolving transient draw simulations, not discussed in this paper, also show that above a certain critical value for an overpressure, which in our case is less than 7Pa, even if the fiber does not blow up immediately, the drawing process never reaches its steady state. A more subtle way of controlling the core collapse is by changing the preform feeding speed, although, for a given draw ratio, this could be limited by the maximal draw velocity.

CONCLUSION

Drawing of multilayer hollow polymer fibers was studied using the thin filament approximation. A Newtonian model for the flow was considered. We have characterized surface tension mitigated core collapse and closely related layer thickness non-uniformity. We have demonstrated that by varying various control parameters such as furnace temperature, feeding speed and pressurization it is possible to reduce hole collapse. While hole pressurization provides a very effective way of compensating for the hollow core collapse, it was found that the final fiber dimensions are very sensitive to the value of an overpressure. Moreover, the draw process could newer reach a steady state if overpressure larger than a certain critical value were used.

AKNOWLEDGEMENTS

Funding for this work comes partially from the contribution of Canada Institute for Photonic Innovations, projects BP5 and FP3.

REFERENCES

1. Katsuyama, T. and Matsumura, H., Infrared Optical Fibers, 1989.
2. Saito, M. and Kikuchi, K., "Infrared optical fiber sensors," Opt. Rev. 4, 527-538 (1997)
3. Sanghera, J. and Aggarwal, I., Infrared Fiber Optics, 1998.
4. S. Martellucci et al., "Optical Sensors and Microsystems : New Concepts, Materials, Technologies" Plenum 2000
5. J.A. Harrington, "A review of IR transmitting, hollow waveguides," Fib. Integr. Opt. 19, 211 (2000)
6. YW Shi, K. Ito, Y. Matsuura, M. Miyagi, "Multiwavelength laser light transmission of hollow optical fiber from the visible to the mid-infrared," Optics Letters 30, 2867-2869 (2005)
7. P. Russell, "Photonic crystal fibers," Science 299, 358-362 (2003)
8. C.M. Smith, N. Venkataraman, M.T. Gallagher, D. Muller, J.A. West, N.F. Borrelli, D.C. Allan, K.W. Koch, "Low-loss hollow-core silica/air photonic bandgap fibre," Nature 424, 657-659 (2003)
9. M.A. van Eijkelenborg, A. Argyros, G. Barton, I.M. Bassett, M. Fellew, G. Henry, N.A. Issa, M.C.J. Large, S. Manos, W. Padden, L. Poladian, J. Zagari, "Recent progress in microstructured polymer optical fibre fabrication and characterisation," Opt. Fiber Techn. 9, 199-209 (2003)
10. T.Katagiri, Y. Matsuura, M. Miyagi, "Photonic bandgap fiber with a silica core and multilayer dielectric cladding," Opt. Lett. 29, 557-559 (2004)
11. B. Temelkuran, S.D. Hart, G. Benoit, J.D. Joannopoulos, Y. Fink, "Hollow photonic bandgap fibers for NIR applications," Nature 420, 650-653 (2002)
12. M. Skorobogatiy, "Efficient anti-guiding of TE and TM polarizations in low index core waveguides without the need of omnidirectional reflector," Optics Letters 30, 2991 (2005)
13. M. Skorobogatiy et al. "Consecutive Solvent Evaporation Technique to Fabricate Polymer Multilayer Hollow Fiber Preforms", submitted.
14. M.R. Matovich and J.R.A. Pearson, "Spinning a molten threadline - Steady-state isothermal viscous flows," Ind. Eng. Chem. Fundam. **,** 512-520 (1969).
15. Y.T. Shah and J.R.A. Pearson, "On the stability of nonisothermal fiber spinning," Ind. Eng. Chem. Fundam. **,** 145-149 (1972).
16. J.A. Burgman "Liquid glass jets in the forming of continuous fibers," Glass Technol. **,** 110-116 (1970).
17. F.T. Geyling, "Basic fluid dynamic consideration in the drawing of optical fibers," Bell Sys. Tech. J. **,** 1011-1056 (1976).
18. B.D. Freeman, M.M. Denn, R. Keunings, G.E. Molau and J. Ramos, "Profile development in drawn hollow tubes," J. Polym. Eng. **,** 171-186 (1986).
19. A.D. Fitt, K. Furusawa, T.M. Monro, C.P. Please and D.J. Richardson, "The mathematical modelling of capillary drawing for holey fibre manufacture," J. Eng. Math. **,** 201-227 (2002).
20. S.C. Xue, R.I. Tanner, G.W. Barton, R. Lwin, M.C.J. Large and L. Poladian, "Fabrication of

microstructured optical fibers — Part I: Problem formulation and numerical modeling of transient draw process," J. Lightw. Technol. **,** 2245-2254 (2005).
21. S.C. Xue, R.I. Tanner, G.W. Barton, R. Lwin, M.C.J. Large and L. Poladian, "Fabrication of microstructured optical fibers — Part II: Numerical modeling of steady-state draw process," J. Lightw. Technol. **,** 2255-2266 (2005).
22. L.J. Cummings, P.D. Howell, "On the evolution of non-axisymmetric viscous fibres with surface tension, inertia and gravity," J. Fluid mech. **,** 361-389 (1999).
23. H.M. Reeve, A.M. Mescher and A.F. Emery, "Investigation of steady-state drawing force and heat transfer in polymer optical fiber manufacturing," Journal of Heat Transfer **,** 236-243 (2004).
24. S. Wu, "Surface and interfacial tensions of polymer melts. II. Poly(methylmethacrylate), poly(n-butylmethacrylate), and polystyrene," J. Phys. Chem. **,** 632-638 (1970).